A comprehensive model for the electric double layer of stepped platinum electrodes

Fröhlich, N.L.; Liu, J.; Ojha, K.; Hagopian, A.; Doblhoff-Dier, K.; Koper, M.T.M.

Citation

Fröhlich, N. L., Liu, J., Ojha, K., Hagopian, A., Doblhoff-Dier, K., & Koper, M. T. M. (2026). A comprehensive model for the electric double layer of stepped platinum electrodes. *Nature Chemistry*. doi:10.1038/s41557-025-02063-9 nature chemistry

Article

https://doi.org/10.1038/s41557-025-02063-9

A comprehensive model for the electric double layer of stepped platinum electrodes

Received: 27 June 2025

Accepted: 17 December 2025

Nicci L. Fröhlich [1,2], Jinwen Liu[1,2], Kasinath Ojha [1], Arthur Hagopian[1], Katharina Doblhoff-Dier [1] & Marc T. M. Koper [1]

Understanding the electric double layer (EDL) of stepped Pt electrodes is crucial for comprehending the reaction environment for electrocatalytically relevant Pt electrodes, which typically comprise a complex mixture of facet orientations, steps and defects. Here we systematically investigate the EDL structure of these surfaces by periodically perturbing (111) terraces by either (110)- or (100)-type steps. We find that the minimum in the differential capacitance $C_{\mathrm{d,min}}$ in 0.1 mM $HClO_4$ is highly structure sensitive. We attribute this observation to inherent differences in affinity for H_2O dissociation between (110) and (100) facets. Using a continuum model, we confirm that the potential of $C_{\mathrm{d,min}}$ ($E_{\mathrm{d,min}}$) closely approximates the potential of zero free charge E_{pzfc} for the (110)-stepped series. Together with ab initio molecular dynamics simulations, we reveal that OH_{ads} at step sites leads to a different step-density-dependent trend between E_{pzfc} and the work function. Our approach yields a unified picture of the EDL structure on stepped Pt surfaces, bridging the gap between model single-crystal surfaces and practically relevant heterogeneous Pt electrodes.

Elucidating the structure of the electric double layer (EDL) of aqueous electrolyte–electrode interfaces is essential for optimizing many important electrochemical processes. Pt electrodes, known for their excellent catalytic properties, are of particular interest. However, electrocatalytically relevant electrodes are typically poly- or nanocrystalline. For such structurally complex surfaces, fundamental EDL studies remain scarce due to the convoluted nature of elucidating specific structure–capacitance relationships. To bridge our understanding of these complex electrocatalytic systems, stepped single-crystal surfaces provide a controlled platform in which heterogeneous sites can be quantitatively introduced. While such an approach has been used extensively in elucidating the electrocatalytic activity of different Pt facets, there have been very few efforts in this direction when it comes to structure-sensitive EDL properties[1–3].

The (differential) double-layer capacitance, C_d, emanates from the structure of the EDL. In the absence of specific adsorption, the classical Gouy–Chapman (GC) model predicts C_d to display a minimum ($C_{\mathrm{d,min}}$) at the potential of zero free charge (E_{pzfc}). For Pt(111), we recently showed that a $C_{\mathrm{d,min}}$ can only be observed at the E_{pzfc} in extremely dilute 0.1 mM $HClO_4$ electrolyte solutions (pH 4). These anomalously low electrolyte concentrations required to observe the GC-predicted $C_{\mathrm{d,min}}$ have been ascribed to a weak attractive ion–surface interaction, which is not chemically specific[4–7]. Other techniques have also been used to measure the E_{pzc} of Pt surfaces, but they either only approximate the E_{pzfc}, by using assumptions or extrapolation, or provide a measurement of the potential of zero total charge[8–10] (see Supplementary Note 2 for a more detailed discussion).

A true understanding of the EDL structure of Pt electrodes must include the effects of varying facets, steps and defects. This is, however, non-trivial as it is now generally agreed on in the literature that only the Pt(111) facet has a potential window in which interfacial H_2O is not dissociated; all other sites, including (110) and (100), induce H_2O dissociation such that H_{ads}, OH_{ads} or both are present at any applied potential[11,12]. Therefore, a real Pt electrode constitutes a combination of ideally polarizable facets and pseudocapacitive surface sites, and the overall differential capacitance should reflect this complexity. Here, we aim to bridge the gap between single-crystalline surfaces and more heterogeneous surfaces by establishing a comprehensive

---

[1] Leiden Institute of Chemistry, Leiden University, Leiden, the Netherlands. [2] These authors contributed equally: Nicci L. Fröhlich, Jinwen Liu.
e-mail: k.doblhoff-dier@lic.leidenuniv.nl; m.koper@lic.leidenuniv.nl

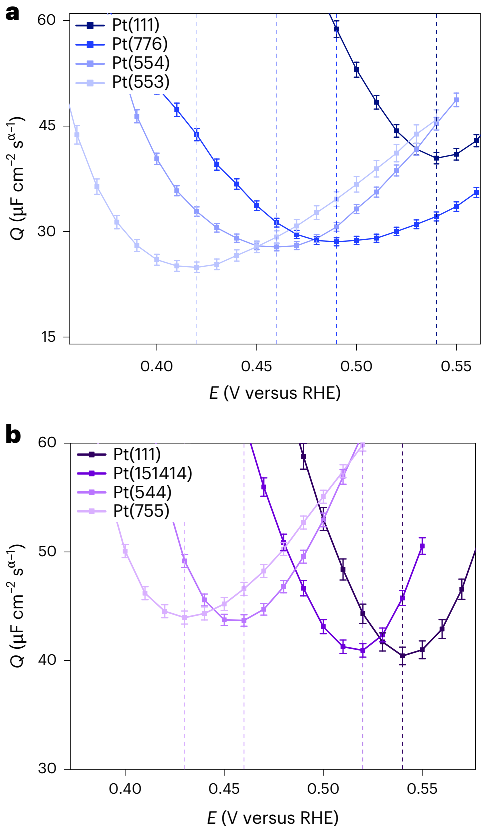

Fig. 1 | Double-layer capacitance curves of stepped Pt electrodes in 0.1 mM $HClO_4$. a,**b**, Capacitance curves for Pt(S)-[(n − 1)(111) × (110)] (n = ∞, 14, 10, 5) (**a**) and Pt(S)-[n(111) × (100)] (n = ∞, 29, 9, 6) (**b**) surfaces measured using EIS (1 kHz to 0.5 Hz, ΔE = 5 mV) fitted with respective serial EECs consisting of a resistor, R, to account for the solution resistance and a CPE, Q, to model the double-layer capacitance (see the Methods for a justification of this choice of EEC as well as Supplementary Figs. 4 and 5 for corresponding CPE exponents, respectively). Data are presented as mean values ± standard deviation of three datasets (Supplementary Note 1).

model for the (structure-sensitive) EDL of high-index single-crystal Pt electrodes. In other words, controlled defects are introduced by diluting the Pt(111) surface with periodic (110)-/(100)-type steps, such that specific structure–capacitance relationships associated with these different step sites can be systematically elucidated.

We reveal that $C_{\mathrm{d,min}}$ is highly structure sensitive in 0.1 mM $HClO_4$, decreasing with increasing (110)-step density, but increasing for (100)-steps. We attribute this step-type-dependent behaviour to the varying affinity of different step orientations for H_2O dissociation[11]: there is a potential-dependent OH_{ads} coverage at (100)-sites within the double-layer window (0.4–0.6 V_{RHE}), whereas this OH_{ads} coverage is potential independent for (110)-step sites. Using ab initio molecular dynamics (AIMD) simulations, assisted by continuum EDL models, we show that the presence of these OH_{ads} leads to a positive shift in the E_{pzfc} relative to the corresponding bare stepped Pt surfaces due to a quenching of the Smoluchowski step dipole and/or a lowering of the step's Helmholtz capacitance.

Results and discussion

Double-layer capacitance of stepped platinum electrodes

Figure 1 shows the differential capacitance data obtained using electrochemical impedance spectroscopy (EIS) for various stepped Pt interfaces in the Pt(111) double-layer window (0.40–0.60 V_{RHE}). Data are obtained for Pt(S)-[(n − 1)(111) × (110)] for n = 14, 10, 5 (Fig. 1a) and for Pt(S)-[n(111) × (100)] for n = 29, 9, 6 (Fig. 1b) in comparison with Pt(111) in 0.1 mM $HClO_4$. The double-layer capacitance is modelled as a constant phase element (CPE, Q); see the Methods for details of equivalent electric circuit (EEC) choice. The corresponding capacitance curves obtained using cyclic voltammetry (CV) as well as the full CVs of these surfaces in a broader potential window are shown in Supplementary Figs. 1–3 (ref. 13).

Consistent with previous results, the differential capacitance of Pt(111) in 0.1 mM $HClO_4$ displays a pronounced minimum at the E_{pzfc} (0.54 V_{RHE}, 0.30 V_{SHE}; Fig. 1)[4,5]. Following the GC theory, this suggests that the capacitance is dominated by the diffuse-layer contribution in this region. Similar minima in the double-layer capacitance can also be observed for the Pt(S)-[(n − 1)(111) × (110)] (n = 14, 10, 5) and Pt(S)-[n(111) × (100)] (n = 29, 9, 6) series in 0.1 mM $HClO_4$ (Fig. 1). We denote the location of these minima as $E_{\mathrm{d,min}}$ and the corresponding capacitance values as $C_{\mathrm{d,min}}$ in the following.

Figure 1 shows that the value of $C_{\mathrm{d,min}}$ is step-density dependent. The value of $C_{\mathrm{d,min}}$ is thus not uniquely defined by the diffuse-layer capacitance, as may be expected in the low concentration limit, but is influenced by the presence of steps. The changes in $C_{\mathrm{d,min}}$ with step density are even step-type dependent: for the Pt(S)-[(n − 1)(111) × (110)] series, $C_{\mathrm{d,min}}$ decreases by ~5 μF cm^{-2} $s^{\alpha-1}$ when increasing the step density from n = ∞ to n = 5 (Fig. 1a). Such a decrease in C_d with increasing (110)-step density was also previously observed by Bandarenka et al., albeit that their data were collected in 0.1 M $HClO_4$, which is fundamentally less meaningful than the data presented here in 0.1 mM $HClO_4$ (see Supplementary Note 3 for more details)[3]. Contrarily, for the Pt(S)-[n(111) × (100)] series, $C_{\mathrm{d,min}}$ increases by ~3 μF cm^{-2} $s^{\alpha-1}$ when increasing the step density from n = ∞ to 6 (Fig. 1b). Similar observations can be made for the capacitance curves obtained from CV (Supplementary Fig. 1).

We interpret this discrepant trend in $C_{\mathrm{d,min}}$ to be a consequence of potential-dependent adsorption processes occurring on only (100)-type steps within the potential region of interest (that is, in the Pt(111) double-layer window, 0.40–0.60 V). To substantiate our claim that these discrepant step-type-dependent trends are a result of the differing nature of adsorption at the respective step sites, we refer to the CVs of the Pt(S)-[(n − 1)(111) × (110)] and Pt(S)-[n(111) × (100)] series at more negative potentials to the potential region of interest (that is, in the 'hydrogen adsorption region'), as well as to Parsons–Zobel (PZ) plots (vide infra).

As shown in Supplementary Figs. 2 and 3, the positive-going blank CVs of the Pt(S)-[(n − 1)(111) × (110)] and Pt(S)-[n(111) × (100)] series display large voltammetric peaks at 0.13 V and 0.30 V, respectively, which intensify with increasing step density[14]. These peaks have been attributed to concurrent exchange of H_{ads} with OH_{ads} at steps (that is, as H_{ads} is de(ad)sorbed, OH_{ads} is simultaneously ad(de)sorbed)[11,12,15]. Therefore, in the Pt(111) double-layer window (0.40–0.60 V), the (110)- and (100)-step sites have a certain (possibly potential-dependent) OH_{ads} coverage, while the (111)-terrace sites remain adsorbate-free.

For the (110)-stepped series, the step-related exchange peak occurs at rather low potentials (0.13 V; Supplementary Fig. 2), far from the potential region of interest (0.40–0.60 V). Similar observations apply to the CV of basal plane Pt(110) (Supplementary Fig. 6), where the pseudocapacitive currents associated with H_{ads}/OH_{ads} exchange occur at relatively low potentials too, leading to a relatively small and constant capacitance (~45 μF cm^{-2}) between 0.40 V and 0.60 V. These observations suggest that (110)-step sites in the Pt(S)-[(n − 1)(111) × (110)] series are probably saturated with a constant OH_{ads} coverage in the potential region of interest.

Conversely, for the (100)-stepped series, the (100)-step-related exchange peak is in much closer proximity (0.30 V; Supplementary Fig. 3) to the (111) double-layer window, implying that, in contrast to (110)-steps, a convolution of adsorption events may occur on (100)-step sites throughout the potential region of interest. The blank CV of the basal plane Pt(100) (Supplementary Fig. 6) supports this claim as there is a large (pseudo-)capacitance (~1,250 μF cm^{-2}) throughout the potential region of interest, consistent with continued H_{ads}/OH_{ads} exchange.

Thus, comparison of the blank CVs for the (110)- and (100)-stepped series with their corresponding basal planes suggests that a changing adsorbate coverage occurs only for (100)-type steps in the potential region of interest, contributing an additional pseudocapacitance that is not observed for (110) steps. This is further corroborated by the respective PZ plots. Details are given in Supplementary Note 4 and Supplementary Fig. 7. The main conclusion is that the PZ plot slope is independent of (110)-step density, whereas a steady decrease in the PZ plot slope is observed with increasing (100)-step density. This decrease in PZ plot slope can only be explained by a non-zero adsorption capacitance at (100)-sites (see Supplementary Note 5 for a derivation), consistent with the step-nature-dependent trends observed in the previously discussed capacitance curves (Fig. 1). We also note that the PZ plot slopes deviate markedly from unity, the value predicted by GC theory and consistent with previous observations for Pt(111)[5,13]. Possible reasons for this anomaly have been discussed in previous work[4,6,16].

If adsorption events indeed take place at the (100)-sites of the Pt(S)-[n(111) × (100)] series in the potential region of interest, this should lead to a capacitance that increases with the step-to-terrace ratio, r_{step} ($r_{\text{step}} = \frac{1}{n}$). If adsorption takes place at the steps, the average total capacitance is expected to behave as

$$C_{\text{tot}} \approx C_{\text{d}} + r_{\text{step}} \times C_{\text{ads}}^{\text{step}}, \tag{1}$$

where C_{d} refers to the capacitance due to the free charge stored at the surface, and $C_{\text{ads}}^{\text{step}}$ refers to the pseudocapacitance caused by adsorption processes at a single step (see Supplementary Note 6 for details). Adsorption events on the steps can thus explain the increasing value of $C_{\text{d,min}}$ for the Pt(S)-[n(111) × (100)] series and the decreased PZ plot slope with increasing step density. It should be noted, however, that the exact origin of the pseudocapacitance observed for the Pt(S)-[n(111) × (100)] series remains unclear. In particular, the pseudocapacitive current observed on basal plane Pt(100) throughout the potential region of interest (that is, >0.40 V; Supplementary Fig. 6) is typically attributed to adsorption occurring on (100)-terrace sites, rather than on (100)-steps, which occurs at more negative potentials (~0.30 V)[17]. Therefore, the pseudocapacitance observed between 0.40 V and 0.60 V for the (100)-stepped series (Fig. 1b) appears unlikely to be explained by concurrent H_{ads}/OH_{ads} on (100)-step sites. Instead, such a pseudocapacitance could be tentatively attributed to H_{ads}/OH_{ads} exchange occurring on a small proportion of (100)-sites that are not monatomically high (that is, step-bunched or defect sites) and therefore resemble adsorption on (100)-terrace sites[18]. An alternative explanation is that OH_{ads} continues to adsorb on (100)-step sites in a potential-dependent manner at potentials positive of the (100)-step exchange peak.

Regardless of the exact origin of pseudocapacitance on (100) sites, the increase in $C_{\text{d,min}}$ taken together with the decreasing PZ-plot slope observed with increasing (100)-step density suggests that it is reasonable to assume that a convoluting adsorption process takes place in the region of interest for the Pt(S)-[n(111) × (100)] series, while this is expected to be absent for the Pt(S)-[(n − 1)(111) × (110)] series. The decrease in $C_{\text{d,min}}$ observed for the Pt(S)-[(n − 1)(111) × (110)] series may instead be caused by a (very) low Helmholtz capacity of the steps, as shown qualitatively in Supplementary Fig. 27 using a continuum model.

Potential of capacitance minimum versus step density

In addition to the trends in $C_{\text{d,min}}$, Fig. 1 reveals that the potential $E_{\text{d,min}}$ at which $C_{\text{d,min}}$ occurs shifts to more negative potentials with increasing step density. For the Pt(S)-[(n − 1)(111) × (110)] series, $E_{\text{d,min}}$ decreases from 0.49 V to 0.46 V and finally to 0.42 V for n = 14, 10 and 5, respectively (Fig. 1a). For the Pt(S)-[n(111) × (100)] series, $E_{\text{d,min}}$ decreases from 0.52 V to 0.46 V to 0.43 V for n = 29, 9 and 6, respectively (Fig. 1b). The same trends can be observed using CV (Supplementary Fig. 1). To understand these trends, we need to assess the factors governing $E_{\text{d,min}}$. We focus on the Pt(S)-[(n − 1)(111) × (110)] series for which C_{d} reflects pure double-layer charging in the region of interest because the OH_{ads} coverage at the step is potential independent, and thus only the free charge capacitance varies (vide supra).

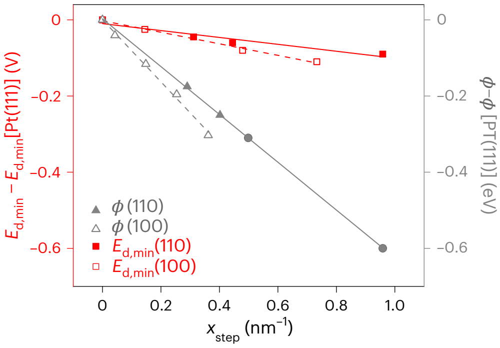

Fig. 2 | Potential of the capacitance minimum and the work function of stepped Pt electrodes as a function of step density. The potential of the capacitance minimum, $E_{\text{d,min}}$, taken from Fig. 1 of Pt(S)-[(n − 1)(111) × (110)] (n = ∞, 14, 10 and 5) (solid squares, slope = −0.009 ± 0.002, R^2 = 0.94) and Pt(S)-[n(111) × (100)] (n = ∞, 29, 9 and 6) (hollow squares, slope = −0.015 ± 0.001, R^2 = 0.99) electrodes measured in 0.1 mM $HClO_4$ using EIS (1 kHz to 0.5 Hz, ΔE = 5 mV, fitted with serial RQ EEC). Data are presented as mean values ± standard deviation of three datasets, but error bars are too small to be visible (Supplementary Note 1). The corresponding work functions, Φ, for Pt(S)-[(n − 1)(111) × (110)] surfaces taken from ref. 24 (solid triangles) and ref. 23 (solid circles, slope −0.06) and Pt(S)-[n(111) × (100)] surfaces (hollow triangles, slope −0.08) taken from ref. 24, respectively, normalized with respect to Pt(111) (Supplementary Table 2). x_{step} corresponds to the nominal step densities calculated according to Supplementary Note 7.

For Pt(111) in 0.1 mM $HClO_4$, $E_{\text{d,min}}$ corresponds to the potential of zero free charge, E_{pzfc} (refs. 4,5). As discussed by Frumkin et al. and Trasatti[19,20], the E_{pzfc} of a material in an aqueous electrochemical environment is expected to be related to the work function, Φ, of the same material in vacuum via[21,22]

$$E_{\text{pzfc}} = \frac{\Phi}{e} + \chi - E_{\text{abs}}(\text{ref}), \tag{2}$$

where e is the electronic charge, χ accounts for the solvation contribution to the surface dipole, and E_{abs}(ref) accounts for the absolute potential of the reference electrode[23].

For stepped Pt surfaces, the work function is known to decrease with step density[23,24] (literature data shown in Fig. 2). This step-induced decrease in Φ has been linked to the Smoluchowski effect: at atomic corrugations, the electronic charge distribution will be smoother than the atomic charge distribution, leading to a spillover of electronic density from the upper step edge to the lower edge. The resulting step dipole is oriented such that it decreases Φ, as illustrated in Supplementary Fig. 12a (ref. 25).

Based on equation (2), the E_{pzfc} is expected to decrease in a similar manner as Φ if χ is approximately independent of the step density. Gomez et al. extracted approximate values for the E_{pzfc} of the Pt(S)-[(n − 1)(111) × (110)] (n > 5) series from CO displacement measurements ($E_{\text{pzfc}}^{\text{CO}}$), which were determined from corresponding potentials of zero total charge, E_{pztc}. These $E_{\text{pzfc}}^{\text{CO}}$ values were indeed found to follow this expected behaviour (that is, agreement with Φ)[8,26]. The $E_{\text{d,min}}$ values extracted from the capacitance minimum in this work also display a linear dependence on step density. However, this dependence is notably weaker than expected based on Φ changes (and therefore also $E_{\text{pzfc}}^{\text{CO}}$; Fig. 2). This either suggests that $E_{\text{d,min}}$ is not equivalent to the E_{pzfc}, or the measurement of $E_{\text{d,min}}$ is fundamentally different from the extrapolated $E_{\mathrm{pzfc}}^{\mathrm{CO}}$ obtained by Gomez et al. We show that this discrepancy cannot be attributed to the former of these two propositions as, using a continuum model, we find a close agreement between $E_{\mathrm{d,min}}$ and E_{pzfc} (vide supra). Instead, we link the discrepancy in the values of $E_{\mathrm{d,min}}$ and $E_{\mathrm{pzfc}}^{\mathrm{CO}}$ to the latter proposition. Specifically, the $E_{\mathrm{pzfc}}^{\mathrm{CO}}$ values obtained by Gomez et al. were extrapolated under the assumption that no $\mathrm{OH_{ads}}$ are present at the step site (that is, the additional charge associated with a given potential-independent $\mathrm{OH_{ads}}$ coverage in the double-layer region was not accounted for), as this idea of $\mathrm{OH_{ads}}$ being present at step sites in the $\mathrm{H_{upd}}$ region was not yet prevailing. However, our measurements do correspond to a surface with $\mathrm{OH_{ads}}$ coverage at the steps. Therefore, the $E_{\mathrm{pzfc}}^{\mathrm{CO}}$ values were calculated on the assumption of an inherently different surface state from that in our measurements. Moreover, in our measurements, the only contribution to the capacitance is a change in the free charge for the (110)-stepped series as no pseudocapacitive current is measured (that is, the $\mathrm{OH_{ads}}$ coverage is potential independent). Therefore, $E_{\mathrm{d,min}}$ must correspond to an E_{pzfc} that is defined in the presence of an equilibrium coverage of $\mathrm{OH_{ads}}$ on the (110)-step sites. In addition, the pH at which these $E_{\mathrm{pzfc}}^{\mathrm{CO}}$ values were obtained reflects a surface also covered in hydrogen adsorbates ($E_{\mathrm{pzfc}} \approx 0.36\ \mathrm{V_{RHE}}$), differing markedly from our measurements of $E_{\mathrm{d,min}}$ here (see Supplementary Note 2 for a more detailed discussion). Therefore, we attribute the unexpectedly reduced slope observed for $E_{\mathrm{d,min}}$ compared with Φ as a function of step density to the presence of adsorbates ($\mathrm{OH_{ads}}$) at the step sites changing the E_{pzfc} (Supplementary Fig. 12b).

Effect of step $\mathrm{OH_{ads}}$ on the potential of zero free charge

To substantiate our claim that the $\mathrm{OH_{ads}}$ at step sites leads to the observed deviation from equation (2), we used a combination of computational models. First, using AIMD simulations, we demonstrate that the presence of $\mathrm{OH_{ads}}$ at the step edges can indeed increase the E_{pzfc} relative to a bare surface and reduce the magnitude of slope of the E_{pzfc} versus x_{step} plot by systematically varying the $\mathrm{OH_{ads}}$ coverage in the simulations. Second, using a continuum model, we prove that the alternative explanation, that is, $E_{\mathrm{d,min}}$ differing from E_{pzfc}, is unlikely. Even for multifaceted surfaces with facet-dependent Helmholtz capacitances, the model predicts $E_{\mathrm{d,min}}$ and E_{pzfc} to be nearly identical, provided that the facet length is much smaller than the Debye length and the adsorbate coverage remains constant across the potential range of interest (expected for Pt(S)-[$(n-1)(111) \times (110)$] surfaces). Furthermore, the continuum model reproduces the reduction in the E_{pzfc} versus x_{step} slope when the Helmholtz capacitance of the step is smaller than that of the terrace, a phenomenon probably related to the presence of $\mathrm{OH_{ads}}$ at the step.

Density functional theory (DFT) and DFT-based AIMD simulations have been performed on the Pt(S)-[$(n-1)(111) \times (110)$] series for $n = 3, 4, 5, 8, 10, \infty$. Computational details of these simulations are provided in Supplementary Notes 9 and 10, and the corresponding Supplementary Figs. 13–20. A representative snapshot for the Pt(553)–$\mathrm{OH_{ads}}$–water interface is shown in Fig. 3a. To investigate the influence of $\mathrm{OH_{ads}}$ at the steps, simulations were carried out with varying $\mathrm{OH_{ads}}$ coverages, and the resulting Φ and E_{pzfc} values were compared. Values for Φ were calculated from static DFT calculations using standard procedures, and values for E_{pzfc} were computed using the computational standard hydrogen electrode method developed by Cheng and Sprik[27–29], as schematically illustrated in Supplementary Fig. 21.

We start by computing the work function of the series of stepped surfaces. As shown in Fig. 3b, the step-induced changes in Φ predicted by DFT are markedly smaller than those observed experimentally. This discrepancy may be caused by errors in our calculations using the generalized gradient approximation functional, as discussed previously and in more detail in Supplementary Note 10 (refs. 30,31). However, regardless of whether experimental or computed Φ values are used, the step-dependent variation in $E_{\mathrm{d,min}}$ is consistently smaller than that in Φ (Fig. 3b).

To further investigate the origin of the discrepant trends of $E_{\mathrm{d,min}}$ and Φ, we computed E_{pzfc} values for the same surfaces using AIMD. In the absence of $\mathrm{OH_{ads}}$ and at low step densities, the computed potential of zero free charge, $E_{\mathrm{pzfc}}^{\mathrm{comp}}$, closely mirrors the trend of the computed Φ (Fig. 3b, dark-red line). At higher step densities (still without $\mathrm{OH_{ads}}$ coverage), differences are observed that we ascribe to the terraces becoming too narrow for the water to behave in a 'terrace-like' manner (Supplementary Fig. 13). When adding $\mathrm{OH_{ads}}$ to the steps, the $E_{\mathrm{pzfc}}^{\mathrm{comp}}$ seems to become substantially noisier. This may be a physical effect in which small changes in ($\mathrm{OH_{ads}}$-covered) step densities cause large changes in the E_{pzfc} but may also be due to a slow equilibration of the $\mathrm{OH_{ads}}$ and surrounding water, leading to potential fluctuations on timescales beyond those sampled by AIMD. A detailed discussion on the sources of error in AIMD is included in Supplementary Note 12. Despite this noise, a clear trend is recovered at high step densities that suggests $\mathrm{OH_{ads}}$ increases the $E_{\mathrm{pzfc}}^{\mathrm{comp}}$ and reduces the $E_{\mathrm{pzfc}}^{\mathrm{comp}}$ versus step density slope. However, due to step bunching that would probably occur under real experimental conditions in the high step density regime[18], no reliable experimental data are available at such high step densities (Supplementary Note 8).

To corroborate the earlier statement that $\mathrm{OH_{ads}}$ at the steps leads to an increase of $E_{\mathrm{pzfc}}^{\mathrm{comp}}$, we computed the Φ versus step density slope separately for different $\mathrm{OH_{ads}}$ coverages by extracting surface and adsorbate configurations from AIMD trajectories (without water) and averaging over snapshots. As shown in Fig. 3c, the results for the bare surfaces align well with the static DFT results in Fig. 3b (solid grey line). $\mathrm{OH_{ads}}$ increases the work function and lowers the absolute value of the Φ versus step density slope. Because $\mathrm{OH_{ads}}$ does not replace interfacial water molecules at low $\mathrm{OH_{ads}}$ coverages (Supplementary Fig. 22), the resulting change in Φ is expected to transfer to E_{pzfc}. A more detailed comparison between the trends in Φ and E_{pzfc} can be found in Supplementary Note 13. These results support our interpretation that the reduced step dependence of $E_{\mathrm{d,min}}$ (corresponding in this case to the E_{pzfc}) compared with Φ arises from the presence of $\mathrm{OH_{ads}}$ at the step sites, which quenches the step dipole associated with the Smoluchowski effect.

Potential of capacitance minimum versus zero free charge

The comparison between the experiments and AIMD calculations was made under the assumption that $E_{\mathrm{d,min}}$ represents the E_{pzfc} of these stepped Pt surfaces. However, given the multisite and adsorbate-covered nature of the stepped surface, the validity of this assumption is under question. To explore this issue, we constructed a continuum model in which the surface comprises two distinct regions or facets, each characterized by its own potential of zero charge ($E_{\mathrm{pzfc}}^{\mathrm{step}}$ and E_{pzfc}^{n111}) and Helmholtz capacitance ($C_{\mathrm{H}}^{\mathrm{step}}$ and C_{H}^{n111}), effectively modelling steps and terraces on a stepped Pt electrode (Fig. 4a and Supplementary Fig. 23) The terrace E_{pzfc} was fixed to the well-established value for Pt(111) ($E_{\mathrm{pzfc}}^{n111} = 0.3\ \mathrm{V}$ vs SHE)[5], while $E_{\mathrm{pzfc}}^{\mathrm{step}} = -0.1\ \mathrm{V}$ vs SHE, reflecting that lower-coordinated surfaces usually have a lower work function[32]. The model is based on a modified Poisson–Boltzmann framework that accounts for asymmetric ion sizes and solvent polarization effects[33–36]. Model details and validation for the single-facet case are provided in Supplementary Note 14 and Supplementary Fig. 24. Limitations of this model are discussed in Supplementary Note 15.

As shown in Fig. 4b, as long as the facet lengths (L) exceed the Debye length of the electrolyte, the model predicts two minima in the capacitance curve, with one at $E_{\mathrm{pzfc}}^{\mathrm{step}}$ and another at $E_{\mathrm{pzfc}}^{\mathrm{terrace}}$. Here, we assumed equal lengths for the step and terrace regions, namely $l_{\mathrm{step}}/L = 0.5$. Under these conditions, $E_{\mathrm{d,min}}$ poorly represents the overall E_{pzfc}. However, as the facet length is reduced, a single minimum is recovered. This is also the case for facet lengths mimicking the steps and terraces in the stepped Pt surfaces considered here—even if a somewhat higher electrolyte concentration than expected based on the experimental conditions is used in the simulations (Supplementary Fig. 25).

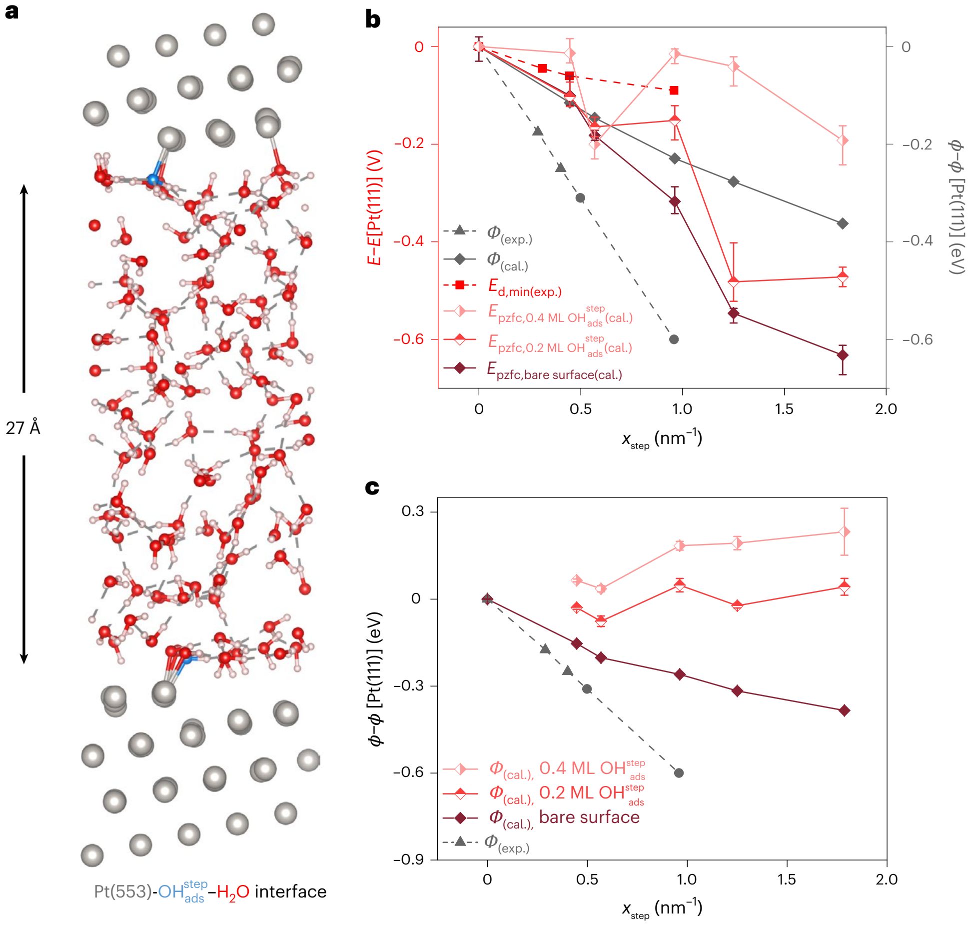

Fig. 3 | Effect of OH adsorbates on the calculated potential of zero free charge and work function of stepped Pt electrodes. a, A representative snapshot during an AIMD simulation for the Pt(553)-OH_{ads}–water interface. **b**, Comparison between the calculated Φ at bare surface and E_{pzfc} at different OH_{ads} coverages on the steps (0, 0.2 and 0.4 ML^{step}; ML = monolayer) normalized by their values of Pt(111) and the experimentally measured Φ (Supplementary Table 2) as a function of x_{step} (calculated according to Supplementary Note 7). The experimentally measured $E_{d,min}$ and work functions, Φ, are the same as those reported in Fig. 2 (solid grey triangle points taken from ref. 24 and solid grey circle points taken from ref. 23). **c**, Calculated average Φ extracted from AIMD trajectories as a function of step density and OH coverage at steps also normalized with respect to those of Pt(111), shown in comparison with the experimentally obtained Φ values[23,24] (also shown in Figs. 2 and 3b). The data in **b** were calculated using the linear regression of water bulk potential versus water bulk density (ρ_{H_2O}) at $\rho_{H_2O} = 1\,g\,cm^{-3}$ ± standard deviation of 12 water bulk regions from this regression, as detailed in Supplementary Note 12. The data in **c** are presented as mean values ± standard deviation over 100 time steps, as shown in Supplementary Fig. 17.

The question remains whether this single $E_{d,min}$ is equivalent to the overall E_{pzfc} of the multifaceted surface.

To model an increasing step density, the ratio between the two facet lengths representing step and terrace is varied. Supplementary Fig. 26 presents the resulting capacitance curves, and Fig. 4c shows the extracted values of $E_{d,min}$ and overall E_{pzfc} as a function of step density. Although $E_{d,min}$ and E_{pzfc} are not identical, their values barely differ when setting the bulk ion concentration to that used in the experiment (0.1 mM). At higher ion concentrations, the discrepancy between $E_{d,min}$ and E_{pzfc} increases, as shown in Fig. 4d. This is consistent with earlier results from Ibach et al. on nanopatterned electrodes in which larger ion concentrations were found to increase the difference between $E_{d,min}$ and E_{pzfc} (ref. 37). Using an ion concentration in the simulations that is higher than the experimental concentration may be reasonable, as previous work has shown that enhanced ion accumulation near the interface can explain the reduced PZ slope on Pt (refs 4,7). At a concentration of 30 mM, which leads to capacitance values in close proximity to those found experimentally (Supplementary Fig. 27), the current model predicts a difference between $E_{d,min}$ and E_{pzfc} of <40 mV for $x_{step} = 1\,nm^{-1}$. This difference is markedly smaller than the deviations observed between $\Delta E_{d,min}$ and $\Delta\Phi$ at the same step density (Figs. 2 and 3c), and it is further diminished when reducing C_H^{step}, as suggested previously to account for the experimentally observed decrease in $C_{d,min}$ with step density. Overall, we cannot exclude a difference between $E_{d,min}$ and E_{pzfc}—especially because our mean-field model is based on rough approximations and parameterizations. Yet, based on the considerations noted earlier, we currently consider it unlikely that a difference between $E_{d,min}$ and E_{pzfc} is the main cause for the differing trends in $\Delta E_{d,min}$ and $\Delta\Phi$ as a function of step density. In any case, the results support the conclusion that the $E_{d,min}$ measured under extremely dilute solution and in the absence of pseudocapacitance is a reasonable approximation of E_{pzfc} for stepped Pt surfaces (Fig. 1a). A more general discussion of the conditions under which $E_{d,min}$ provides a good approximation of E_{pzfc} will be presented in a separate study.

Figure 4c,d also reveals that a sufficiently small C_H^{step} notably suppresses the slope of E_{pzfc} (and $E_{d,min}$) with respect to step density. This behaviour arises because a low C_H effectively 'shields' the contribution of E_{pzc} at this facet. As C_H^{step} approaches zero, the pure terrace behaviour E_{pzfc}^{n111} is recovered and the E_{pzfc} remains constant as a function of step density. A low C_H^{step} (as postulated earlier based on the step dependence of $C_{d,min}$) is thus an alternative explanation for the reduced slope in $E_{d,min}$ compared with Φ as a function of step density.

A low C_H^{step} could be caused by (a) the lower step edge that cannot be closely approached by water (Supplementary Fig. 13) or (b) by the

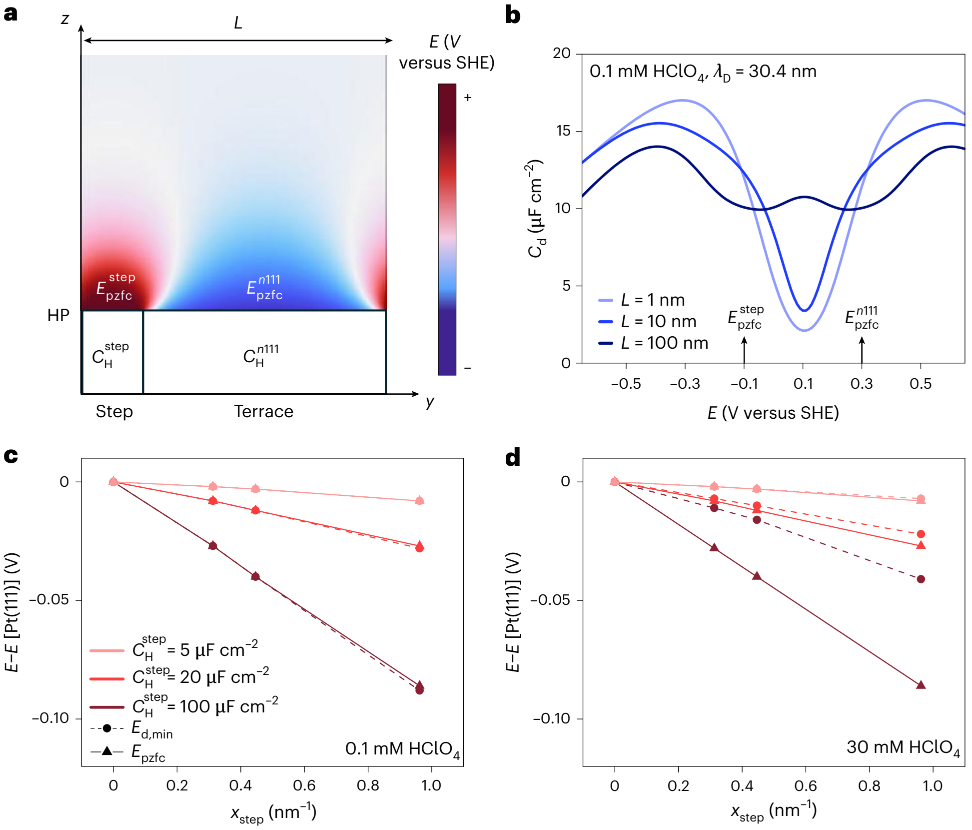

Fig. 4 | Comparison of the potential of capacitance minimum and potential of zero free charge using a continuum model. a, Schematic diagram of potential distribution at E_{pzc} of the overall surface for modelling the surface as consisting of two distinct parts, each characterized by a different E_{pzfc} and Helmholtz capacitance (C_H). HP, Helmholtz plane. **b**, Simulated potential-dependent differential capacitance for different facet lengths L (x nm) at 0.1 mM HClO$_4$ solution. $l_{step}/L = 0.5$, $C_H^{n111} = C_H^{step} = 25\,\mu$F cm^{-2}; other parameters are listed in Supplementary Table 3. **c**,**d**, Comparison of potential of capacitance minimum ($E_{d,min}$) and potential of zero free charge (E_{pzfc}) normalized to that of Pt(111) as a function of step density and C_H^{step} in 0.1 mM (**c**) and 30 mM (**d**) HClO$_4$ solution. $C_H^{n111} = 100\,\mu$F cm^{-2}. The circle markers connected by dashed lines are $E_{d,min}$, while triangle markers connected by solid lines are E_{pzfc}.

adsorbates at the step. The presence of CO on surfaces, has been shown, for example, to markedly reduce the capacitance[38]. Based on our AIMD simulations, which show no deviation between $\Delta\Phi$ and ΔE_{pzfc} on bare stepped surfaces at low step density, we refute option (a). We cannot, however, exclude option (b), which would be consistent with our earlier assertion that the deviating trend between $E_{d,min}$ and Φ as a function of step density is adsorbate induced.

In summary, the observed dependence of E_{pzfc} on step density can, in principle, have two interpretations: (1) as x_{step} increases, the contribution of the step OH$_{ads}$ increases simultaneously, leading to a reduced slope in E_{pzfc} compared with Φ; (2) C_H^{step} is very low (due to the presence of OH$_{ads}$), meaning that the E_{pzfc} is dominated by the (111)-terrace, in which case the implication would be that E_{pzfc}^{n111} is dependent on terrace width, n. This latter proposition cannot be excluded as a possibility using our current model.

Conclusion

In this Article, we have investigated the capacitance trends for two series of stepped Pt electrodes (Pt(S)-[(n − 1)(111) × (110)] and Pt(S)-[n(111) × (100)]) in the Pt(111) double-layer window (0.40–0.60 V$_{RHE}$) at low electrolyte concentrations. While both stepped Pt series displayed a capacitance minimum, $C_{d,min}$, analogous to the one previously observed for Pt(111) at the potential of zero free charge, E_{pzfc}, $C_{d,min}$ was found to be structure sensitive: $C_{d,min}$ increases with increasing (100)-step density, but decreases for the (110)-series. This was rationalized by the differing affinity of these respective step sites for potential-dependent H$_2$O dissociation: OH$_{ads}$ coverage on (110)-steps is effectively potential independent in the potential region of interest, yielding pure double-layer behaviour (albeit in the presence of adsorbates), whereas a convoluting adsorption capacitance was measured for (100)-steps, probably due to a potential-dependent OH$_{ads}$ coverage.

Furthermore, the potential at which $C_{d,min}$ occurs, $E_{d,min}$, linearly decreases with increasing step density, in agreement with work function, Φ, trends but with a much weaker step-density dependence. AIMD simulations show that this reduced step-density dependence of $E_{d,min}$ could be caused by the presence of OH$_{ads}$ at the step site, quenching the Smoluchowski dipole. Alternatively, a continuum EDL model shows that the reduced step-density dependence could be caused by a lower Helmholtz capacitance at the step, quenching the influence of the step on the overall potential of zero charge. The model also confirms that $E_{d,min}$ coincides closely with the E_{pzfc} of the total stepped Pt surface if the adsorbate coverage is potential independent in the potential region of interest.

In summary, we have presented here a comprehensive, detailed and quantitative picture of the highly structure-sensitive electrical double-layer structure at stepped Pt electrodes, highlighting the non-trivial nature of adsorption to the overall capacitance measured. These insights will be important in correctly interpreting the double-layer properties of more structurally complex but practically relevant Pt surfaces.

Online content

Any methods, additional references, Nature Portfolio reporting summaries, source data, extended data, supplementary information, acknowledgements, peer review information; details of author contributions and competing interests; and statements of data and code availability are available at https://doi.org/10.1038/s41557-025-02063-9.

References

1. Koper, M. T. M. Structure sensitivity and nanoscale effects in electrocatalysis. *Nanoscale* **3**, 2054–2073 (2011).
2. Feliu, J. M. & Herrero, E. Pt single crystal surfaces in electrochemistry and electrocatalysis. *EES Catal.* **2**, 399–410 (2024).
3. Xue, S. et al. Impact of Pt(*hkl*) electrode surface structure on the electrical double layer capacitance. *J. Am. Chem. Soc.* **146**, 3883–3889 (2024).
4. Ojha, K., Doblhoff-Dier, K. & Koper, M. T. M. Double-layer structure of the Pt(111)–aqueous electrolyte interface. *Proc. Natl Acad. Sci. USA* **119**, e2116016119 (2022).
5. Ojha, K., Arulmozhi, N., Aranzales, D. & Koper, M. T. M. Double layer at the Pt(111)–aqueous electrolyte interface: potential of zero charge and anomalous Gouy–Chapman screening. *Angew. Chem. Int. Ed.* **59**, 711–715 (2020).
6. Doblhoff-Dier, K. & Koper, M. T. M. Electric double layer of Pt(111): known unknowns and unknown knowns. *Curr. Opin. Electrochem.* **39**, 101258 (2023).
7. Doblhoff-Dier, K. & Koper, M. T. M. Modeling the Gouy–Chapman diffuse capacitance with attractive ion–surface interaction. *J. Phys. Chem. C* **125**, 16664–16673 (2021).
8. Climent, V., Attard, G. A. & Feliu, J. M. Potential of zero charge of platinum stepped surfaces: a combined approach of CO charge displacement and N_2O reduction. *J. Electroanal. Chem.* **532**, 67–74 (2002).
9. Martínez-Hincapié, R., Climent, V. & Feliu, J. M. Investigation of the interfacial properties of platinum stepped surfaces using peroxodisulfate reduction as a local probe. *Electrochim. Acta* **307**, 553–563 (2019).
10. García-Aráez, N., Climent, V. & Feliu, J. M. Potential-dependent water orientation on Pt(111) stepped surfaces from laser-pulsed experiments. *Electrochim. Acta* **54**, 966–977 (2009).
11. Rizo, R. et al. Analysis of the OH coverage on low-coordinated Pt sites at low potentials. *ACS Electrochem.* **1**, 351–359 (2025).
12. Rizo, R. et al. Investigating the presence of adsorbed species on Pt steps at low potentials. *Nat. Commun.* **13**, 2550 (2022).
13. Fröhlich, N. L., Eggebeen, J. J. J. & Koper, M. T. M. Measurement of the double-layer capacitance of Pt(111) in acidic conditions near the potential of zero charge. *Electrochim. Acta* **494**, 144456 (2024).
14. Rizo, R., Herrero, E., Climent, V. & Feliu, J. M. On the nature of adsorbed species on platinum single crystal electrodes. *Curr. Opin. Electrochem.* **38**, 101240 (2023).
15. van der Niet, M. J. T. C., Garcia-Araez, N., Hernández, J., Feliu, J. M. & Koper, M. T. M. Water dissociation on well-defined platinum surfaces: the electrochemical perspective. *Catal. Today* **202**, 105–113 (2013).
16. Huang, J. Zooming into the inner Helmholtz plane of Pt(111)–aqueous solution interfaces: chemisorbed water and partially charged ions. *JACS Au* **3**, 550–564 (2023).
17. Chen, X., Ojha, K. & Koper, M. T. M. Deconvolution of the voltammetric features of a Pt(100) single-crystal electrode. *J. Phys. Chem. Lett.* **15**, 4958–4964 (2024).
18. Valls Mascaró, F., Koper, M. T. M. & Rost, M. J. Step bunching instability and its effects in electrocatalysis on platinum surfaces. *Nat. Catal.* **7**, 1165–1172 (2024).
19. Emets, V. V. & Damaskin, B. B. The relation between the potential of zero charge and work function for sp-metals. *Russ. J. Electrochem.* **45**, 45–57 (2009).
20. Frumkin, A., Damaskin, B., Bagotskaya, I. & Grigoryev, N. Potentials of zero charge, interaction of metals with water and adsorption of organic substances—II. Potentials of zero charge and the work function. *Electrochim. Acta* **19**, 75–81 (1974).
21. Trasatti, S. in *Comprehensive Treatise of Electrochemistry: The Double Layer* (eds Bockris, J. O., Conway, B. E. & Yeager, E.) 45–81 (Springer, 1980).
22. Trasatti, S. Work function, electronegativity, and electrochemical behaviour of metals: II. Potentials of zero charge and 'electrochemical' work functions. *J. Electroanal. Chem. Interfacial Electrochem.* **33**, 351–378 (1971).
23. Ross, P. N. The role of defects in the specific adsorption of anions on Pt(111). *J. Chim. Phys.* **88**, 1353–1380 (1991). & Jr.
24. Besocke, K., Krahl-Urban, B. & Wagner, H. Dipole moments associated with edge atoms; a comparative study on stepped Pt, Au and W surfaces. *Surf. Sci.* **68**, 39–46 (1977).
25. Smoluchowski, R. Anisotropy of the electronic work function of metals. *Phys. Rev.* **60**, 661–674 (1941).
26. Frumkin, A. N. & Petrii, O. A. Potentials of zero total and zero free charge of platinum group metals. *Electrochim. Acta* **20**, 347–359 (1975).
27. Cheng, J. & Sprik, M. Alignment of electronic energy levels at electrochemical interfaces. *Phys. Chem. Chem. Phys.* **14**, 11245–11267 (2012).
28. Cheng, J., Liu, X., VandeVondele, J., Sulpizi, M. & Sprik, M. Redox potentials and acidity constants from density functional theory based molecular dynamics. *Acc. Chem. Res.* **47**, 3522–3529 (2014).
29. Le, J., Iannuzzi, M., Cuesta, A. & Cheng, J. Determining potentials of zero charge of metal electrodes versus the standard hydrogen electrode from density-functional-theory-based molecular dynamics. *Phys. Rev. Lett.* **119**, 16801 (2017).
30. Bramley, G., Nguyen, M.-T., Glezakou, V.-A., Rousseau, R. & Skylaris, C.-K. Reconciling work functions and adsorption enthalpies for implicit solvent models: a Pt (111)/Water interface case study. *J. Chem. Theory Comput.* **16**, 2703–2715 (2020).
31. De Waele, S., Lejaeghere, K., Sluydts, M. & Cottenier, S. Error estimates for density-functional theory predictions of surface energy and work function. *Phys. Rev. B* **94**, 235418 (2016).
32. Li, P., Liu, Y. & Chen, S. Microscopic EDL structures and charge–potential relation on stepped platinum surface: Insights from the ab initio molecular dynamics simulations. *J. Chem. Phys.* **156**, 104701 (2022).
33. de Kam, L. B. T., Maier, T. L. & Krischer, K. Electrolyte effects on the alkaline hydrogen evolution reaction: a mean-field approach. *Electrochim. Acta* **497**, 144530 (2024).
34. Iglič, A., Gongadze, E. & Kralj-Iglič, V. Differential capacitance of electric double layer—influence of asymmetric size of ions, thickness of stern layer and orientational ordering of water dipoles. *Acta Chim Slov* **66**, 534–541 (2019).
35. Liu, J. & Huang, J. A mean-field model for the double layer of stepped platinum single-crystal electrodes. *J. Electroanal. Chem.* **846**, 113136 (2019).
36. Zhang, L., Chen-Kun, L. & Huang, J. A Beginners' guide to modelling of electric double layer under equilibrium, nonequilibrium and AC conditions. *J. Electrochem.* **28**, 2108471 (2022).
37. Ibach, H., Beltramo, G. & Giesen, M. Interface capacitance of nano-patterned electrodes. *Surf. Sci.* **605**, 240–247 (2011).
38. Sundararaman, R., Figueiredo, M. C., Koper, M. T. M. & Schwarz, K. A. Electrochemical capacitance of CO-terminated Pt(111) dominated by the CO–solvent gap. *J. Phys. Chem. Lett.* **8**, 5344–5348 (2017).

Methods

Experimental

The electrochemical glassware cleaning procedure, CV and EIS measurements, and the Ohmic drop compensation method used in this study were performed following previously outlined protocols[13,39]. Disc-type Pt(111) (diameter 3 mm, MaTeck, 99.999%), Pt(S)-[$(n-1)$(111) × (110)] electrodes with $n = 14, 10, 5$ (diameter 4 mm, MaTeck, 99.999%) and Pt(S)-[n(111) × (100)] electrodes with $n = 29, 9, 6$ (diameter 4 mm, Surface Preparation Laboratory and Mateck, 99.999%, respectively) were used as the working electrodes. All the potentials in this Article are reported versus the reversible hydrogen electrode (RHE) scale and have been appropriately Ohmic drop corrected. For further details and explanation of the choice of parameters in CV and EIS measurements, see ref. 13.

Choice of EEC when fitting EIS data

The measured double-layer capacitance, C_d, displays a frequency-dependent real impedance for all surfaces studied here, consistent with previous observations[13]. In principle, C_d must therefore be modelled by a CPE (Q_d) rather than an ideal capacitor (connect in series with a resistor to model the solution resistance R, that is, a serial connection of R and CPE, RQ EEC)[13]. However, the deviations we find between Q_d extracted from impedance measurements (Fig. 1) and C_d extracted directly from the CVs (Supplementary Fig. 1) are small as the CPE exponents, α, which quantify the extent of CPE behaviour, range between 0.95 and 0.99 (Supplementary Figs. 4 and 5)[40,41]. Therefore, although the numerical values deviate slightly from one another due to the presence of this CPE behaviour, Q_d and C_d can be used essentially interchangeably as the capacitance behaviour is nearly perfect.

DFT calculations

Periodic DFT calculations were conducted to determine the work function of a series of 110-type stepped Pt surfaces, Pt(S)-[$(n-1)$(111) × (110)], with $n = 3, 4, 5, 8$ and 10, corresponding to Pt(331), Pt(221), Pt(553), Pt(443) and Pt(554), respectively. The Pt(111) surface ($n = \infty$) was also modelled as a reference. The calculations were carried out using the Vienna Ab initio Simulation Package (VASP)[42–44]. A plane-wave basis set with a cut-off energy of 400 eV was used, and the core electrons were treated using the projector augmented wave (PAW) method (PAW_PBE 04.Feb.2005 for Pt)[45,46]. The Perdew–Burke–Ernzerhof (PBE) exchange-correlation functionals was used, with the Grimme D3 method applied to account for the van der Waals dispersion corrections. The rationale for this choice of functional is discussed in Supplementary Note 10. The optimized lattice constant of bulk Pt obtained using PBE-D3 is 3.92 Å, which agrees with the experimental value of 3.92 Å (ref. 47).

All surfaces were modelled using a six-layer slab, with the bottom layer fixed. The detailed lattice parameters for all surfaces are provided in Supplementary Table 1. A vacuum region of 20 Å was included between metal slabs to limit the surface–surface interactions. Dipole corrections were applied along the surface normal direction. The k-point meshes (k_1, k_2, k_3) were chosen such that their product with the norms of the lattice vectors (a_1, a_2, a_3) satisfied the condition (a_1k_1, a_2k_2, a_3k_3) > (45 Å, 45 Å, 30 Å).

AIMD calculations

AIMD calculations were performed to compute the E_{pzfc} using the CP2K package[48]. The surface dimensions were consistent with those described earlier, but water molecules were introduced between metal slabs of about 27 Å to create a sufficiently long water bulk region with a density of 1 g cm^{-3}, as detailed in Supplementary Table 1 and Supplementary Fig. 13. During the AIMD, the inner two metal layers are fixed while the other layers are relaxed. The Gaussian basis sets used were double-ζ with one set of polarization functions (DZVP-MOLOPT-SR-GTH for H and O and DZVP-A5-Q10-323-MOL-T1-DERIVED_SET-1 for Pt)[49]. An energy cut-off of 400 Ry was applied, and core electrons were modelled using Goedecker–Teter–Hutter pseudopotentials (O: GTH-PBE-q6, H:GTH-PBE-q1, Pt:GTH-PBE-q10)[49,50]. Due to the large size of the unit cells, the interface is simulated at the Γ point in reciprocal space. To account for differences in k-point sampling and basis sets, a correction term was applied when calculating the E_{pzfc} by comparing work function values obtained from VASP (with k-point sampling) and CP2K (without k-point sampling). The second-generation Car–Parrinello molecular dynamics (SGCPMD) was used to sample the Pt–water interfaces at a target temperature of 330 K. The Langevin friction coefficient (γ_L) and intrinsic friction coefficients (γ_D) were chosen to be consistent with previous studies[51–53], with values of $\gamma_L = 0.001\,\mathrm{fs}^{-1}$, $\gamma_D^{H_2O} = 2.2\times10^{-4}\,\mathrm{fs}^{-1}$ and $\gamma_D^{Pt} = 5\times10^{-5}\,\mathrm{fs}^{-1}$. As shown in Supplementary Fig. 15, the temperature of all stepped Pt–water interfaces converged around the target temperature. Detailed set-up information for SGCPMD can be found in refs. 51–53.

The Pt–water interfaces were pre-equilibrated using classical molecular dynamics for 1 ns, and the resulting structures were used as initial configurations for AIMD simulations. All the AIMD simulations were sampled for 15–20 ps with a time step of 0.5 fs to ensure proper equilibration, considering the initial 5 ps (10,000 steps) as an equilibration period and the later 10–15 ps as a production period.

Continuum model

A modified Poisson–Boltzmann equation that considers the effect of asymmetric ion size[36] and solvent polarization[33] was used to simulate the double layer of stepped Pt electrodes. The model was solved in COMSOL Multiphysics 6.2. Model equations and parameters are detailed in Supplementary Note 14.

Data availability

All data underlying this publication will be made available via data.4tu.nl at https://doi.org/10.4121/0d36fb42-5202-4607-ba63-0ed40da2daf2 upon publication. Source data are provided with this paper.

References

39. Fröhlich, N. et al. Effect of trace impurities in perchloric acid on blank voltammetry of Pt(111). *Electrochim. Acta* **466**, 143035 (2023).
40. Lasia, A. The origin of the constant phase element. *J. Phys. Chem. Lett.* **13**, 580–589 (2022).
41. Lazanas, A. C. & Prodromidis, M. I. Electrochemical impedance spectroscopy—a tutorial. *ACS Meas. Sci. Au* **3**, 162–193 (2023).
42. Kresse, G. & Furthmüller, J. Efficiency of ab-initio total energy calculations for metals and semiconductors using a plane-wave basis set. *Comput. Mater. Sci.* **6**, 15–50 (1996).
43. Kresse, G. & Hafner, J. Ab initio molecular dynamics for liquid metals. *Phys. Rev. B* **47**, 558–561 (1993).
44. Kresse, G. & Furthmüller, J. Efficient iterative schemes for ab initio total-energy calculations using a plane-wave basis set. *Phys. Rev. B* **54**, 11169–11186 (1996).
45. Blöchl, P. E. Projector augmented-wave method. *Phys. Rev. B* **50**, 17953–17979 (1994).
46. Kresse, G. & Joubert, D. From ultrasoft pseudopotentials to the projector augmented-wave method. *Phys. Rev. B* **59**, 1758–1775 (1999).
47. Kittel, C. *Introduction to Solid State Physics* (John Wiley and Sons, 2005).
48. VandeVondele, J. et al. Quickstep: fast and accurate density functional calculations using a mixed Gaussian and plane waves approach. *Comput. Phys. Commun.* **167**, 103–128 (2005).
49. VandeVondele, J. & Hutter, J. Gaussian basis sets for accurate calculations on molecular systems in gas and condensed phases. *J. Chem. Phys.* **127**, 114105 (2007).
50. Goedecker, S., Teter, M. & Hutter, J. Separable dual-space Gaussian pseudopotentials. *Phys. Rev. B* **54**, 1703–1710 (1996).

51. Fogarty, R. M., Li, B. X., Harrison, N. M. & Horsfield, A. P. Structure and interactions at the Mg(0001)/water interface: an ab initio study. *J. Chem. Phys.* **156**, 244702 (2022).
52. Chen, A., Le, J.-B., Kuang, Y. & Cheng, J. Modeling stepped Pt/water interfaces at potential of zero charge with ab initio molecular dynamics. *J. Chem. Phys.* **157**, 94702 (2022).
53. Le, J.-B., Fan, Q.-Y., Li, J.-Q. & Cheng, J. Molecular origin of negative component of Helmholtz capacitance at electrified Pt(111)/water interface. *Sci. Adv.* **6**, eabb1219 (2020).

Acknowledgements

N.L.F., J.L., A.H., K.D.D. and M.T.M.K. received funding from the European Research Council (ERC) (advanced grant no. 101019998 'FRUMKIN'). J.L. and K.D.D. acknowledge NWO for providing computational resources: This publication is part of the project 'Computational Electrochemistry' with file number 2025.014 of the research programme 'Computing Time on National Computer Facilities', which is (partly) financed by the Dutch Research Council (NWO) under the grant https://doi.org/10.61686/BOKDD81349. J.L. would like to thank J. Le for helpful discussions on AIMD simulations, and J. Huang, Y. Zhang and K. Levey for their valuable insights on the continuum model.

Author contributions

N.L.F., J.L., K.D.D. and M.T.M.K. conceived the project and wrote the manuscript. N.L.F., K.O. and M.T.M.K. designed the electrochemical experiments. N.L.F. carried out electrochemical characterization. K.D.D. and J.L. designed the simulations. J.L. carried out the DFT-based AIMD simulations and the continuum modelling, under supervision of M.T.M.K., K.D.D. and A.H. All authors read and commented on the manuscript. All authors approved the final version of the manuscript.

Competing interests

The authors declare no competing interests.

Additional information

Supplementary information The online version contains supplementary material available at https://doi.org/10.1038/s41557-025-02063-9.

Correspondence and requests for materials should be addressed to Katharina Doblhoff-Dier or Marc T. M. Koper.

Peer review information *Nature Chemistry* thanks Victor Climent, Kathleen Schwarz and the other, anonymous, reviewer(s) for their contribution to the peer review of this work.